UNIVERSITÄT AUGSBURG
Universitätsbibliothek

OPEN ACCESS
OPUS AUGSBURG

Compensation of plasma fluctuation induced shadowing effects in gas puff imaging data

M. Griener, J. Kalis, D. Wendler, Gregor Birkenmeier, E. Wolfrum, R. M. McDermott, U. Stroth

Angaben zur Veröffentlichung / Publication details:

Griener, M., J. Kalis, D. Wendler, Gregor Birkenmeier, E. Wolfrum, R. M. McDermott, and U. Stroth. 2023. "Compensation of plasma fluctuation induced shadowing effects in gas puff imaging data." *Nuclear Materials and Energy* 34: 101346. https://doi.org/10.1016/j.nme.2022.101346.

Nutzungsbedingungen / Terms of use:

CC BY-NC-ND 4.0

Dieses Dokument wird unter folgenden Bedingungen zur Verfügung gestellt: / This document is made available under these conditions:
CC-BY-NC-ND 4.0: Creative Commons: Namensnennung - Nicht kommerziell - Keine Bearbeitung
Weitere Informationen finden Sie unter: / For more information see:
https://creativecommons.org/licenses/by-nc-nd/4.0/deed.de

Nuclear Materials and Energy 34 (2023) 101346

Contents lists available at ScienceDirect

Nuclear Materials and Energy

journal homepage: www.elsevier.com/locate/nme

Compensation of plasma fluctuation induced shadowing effects in gas puff imaging data

M. Griener [a,*], J. Kalis [a,b], D. Wendler [a,b], G. Birkenmeier [a,b], E. Wolfrum [a], R.M. McDermott [a], U. Stroth [a,b], the ASDEX Upgrade Team[1], the EUROfusion MST1 Team[2]

[a] Max Planck Institute for Plasma Physics, Boltzmannstr. 2, 85748 Garching, Germany
[b] Physik Department E28, Technische Universität München, 85748 Garching, Germany

ARTICLE INFO

Keywords:
Fusion
Plasma edge
Plasma modes
EDA H-mode
Quasi-coherent mode
Plasma filaments
Edge turbulence
Active spectroscopy
Gas puff imaging
Shadowing effects
Helium beam diagnostic
Line ratios

ABSTRACT

For gas puff imaging (GPI) studies of turbulent processes in the plasma edge, it is often assumed that the emitted light is mainly proportional to the local electron density. This, however, only holds for low electron densities in the far scrape-off layer. As GPI typically only detects one emission line, data interpretation further inside the plasma (i.e. around the separatrix) is complicated by two effects. First, there is the strongly non-linear connection between plasma temperature and density and the measured line emission. This can lead to incorrect data interpretation such as an artificial doubling of the frequency of periodic plasma perturbations. Second, a shadowing effect in the neutral distribution can hamper the localization of turbulent structures and modes. For this study thermal helium beam data of an ASDEX Upgrade EDA H-mode scenario are analyzed. By comparing these measurements to a synthetic diagnostic, we demonstrate the presence of diagnostic effects and illustrate their origins. It is shown that when line intensity ratios are used for the analysis, instead of emission from individual lines, the underlying plasma dynamics can be well recovered.

1. Introduction

Active spectroscopy is a common method to diagnose magnetically confined plasmas. It is based on the interaction of the main plasma or its impurities with either high energy beams or locally injected gas. A common representative of the second kind is the gas puff imaging (GPI) diagnostic (see [1] for a comprehensive review), utilizing either deuterium or helium as injected gas. The high temporal resolution on the order of 1 MHz allows these diagnostics to be used for turbulence analysis in the plasma edge. In the far scrape-off layer (SOL) it can be assumed that the emitted light of one selected wavelength (either D_α at 656.3 nm for deuterium or the 587.6 nm or 667.8 nm He I lines) is mainly proportional to the local electron density [1]. However, as the electron densities (n_e) and temperatures (T_e) increase toward the separatrix, this direct proportionality no longer holds.

Two main effects, which are often neglected, can disturb the direct interpretation of the data [2]. First, the non-linear connection between plasma n_e and T_e and the observed emission intensity and second, shadowing effects caused by an inhomogeneous neutral distribution due to ionization losses of the spectroscopy gas. These effects become important on short time scales of the turbulence propagation speed (several microseconds) because the neutral propagation speed is of the same order [1]. To resolve the quantitative influence of these effects, the comparison of measurements with simulations is needed. Important progress in simulating deuterium GPI was done in [2,3], where the DEGAS 2 Monte Carlo neutral transport code was used to implement a synthetic GPI diagnostic in Alcator C-Mod. For a quantitative description, the code needs to handle different excitation mechanisms such as electron excitation and electron dissociation, which is dominant in the far SOL [4]. Furthermore, ionization losses need to be considered to treat shadowing effects by a time-dependent variability in the GPI neutral gas cloud for distances greater than one mean free path from the gas source [3]. However, as stated in [3], the experimental implications of these findings were not clear as no direct comparison of simulation and experiment was done. The same holds for study [4], which uses a drift-reduced Braginskii model for the plasma and a kinetic model for the neutral distribution to generate a synthetic GPI diagnostic in slab geometry. It includes a full model for D_α emission from D excitation as well as D_2 and D_2^+ dissociation, recombination is not included yet. The

* Corresponding author.
E-mail address: Michael.Griener@ipp.mpg.de (M. Griener).
[1] See author list of "STROTH, U. et al., Nuclear Fusion **62** (2022) 042006".
[2] See author list of "LABIT, B. et al., Nucl. Fusion **59** (2019) 086020".

https://doi.org/10.1016/j.nme.2022.101346
Received 30 June 2022; Received in revised form 14 October 2022; Accepted 19 December 2022
Available online 22 December 2022
2352-1791/© 2022 The Author(s). Published by Elsevier Ltd. This is an open access article under the CC BY-NC-ND license (http://creativecommons.org/licenses/by-nc-nd/4.0/).

work reinforces the initial statement that D_α emission is not always directly proportional to n_e by demonstrating its correlation with n_e and T_e along the plasma radius [4]. Furthermore, it shows the anti-correlation of the emission with n_e and T_e at high temperatures and densities inside the separatrix, by considering the influence of the neutral distribution.

In this paper, measurements from the thermal helium beam diagnostic (THB) at ASDEX Upgrade (AUG) are compared to modeled emission patterns in an EDA H-mode scenario [5], with a focus on the dynamics of the quasi-coherent mode with a frequency of 29 kHz. The THB can be considered as a multi-color GPI system for He I lines. By building a synthetic model of the diagnostic we demonstrate the presence of effects that appear when the emission of only one wavelength is analyzed, as typically done within GPI. It is demonstrated how these effects can be overcome when more than one wavelength is used for the analysis and how conclusions can be drawn even without applying a full collisional-radiative model (CRM) as is used to reconstruct plasma profiles.

The paper is organized as follows: In Section 2, the experimental capabilities of the THB are introduced and possible evaluation methods as well as the achievable spatial resolution is discussed. By means of a CRM the influence of the neutral distribution is highlighted and the sensitivity and response of measurement signals to changes in n_e and T_e are demonstrated. In Section 3 data from a synthetic diagnostic is shown and compared to experimental measurements. This comparison highlights features of the measurement that can lead to misinterpretations of the data when only a single wavelength is measured. Section 4 concludes this paper, showing that with the appropriate tools and awareness of possible diagnostic effects, helium beam spectroscopy is an ideal tool for analyzing fast modes and turbulent filaments in the plasma edge region.

2. Basics of helium beam line emission

2.1. Thermal helium beam diagnostics at AUG

The thermal helium beam diagnostic (THB) at AUG delivers electron temperature and density data simultaneously over a wide radial region from just inside the separatrix up to the far SOL. For the measurement, helium is locally injected with an in-vessel piezo valve [6] and fast chopping of the gas inlet allows background subtraction. The typical puff duration is 50 ms with a 10 Hz repetition rate. The emission intensities of four neutral helium lines (587 nm, 667 nm, 706 nm and 728 nm) are measured simultaneously by a 32-channel polychromator system with a temporal resolution of 900 kHz. A spatial resolution of 3 mm is achieved due to the careful parallel alignment of the lines of sight (LOS) to the magnetic field lines at the measurement position. A detailed description of the measurement setup can be found in [7].

The AUG He beam uses a He injection rate of 2×10^{19} particles per second, which is around a factor of 10 smaller compared to the AUG GPI system [8]. The lower gas rate is sustainable due to the higher light transmission and detection efficiency. At this rate we do not observe any perturbation of the plasma, enabling the He beam to be operated as a routine diagnostic.

2.2. Evaluation methods of He-beam measurements

To derive n_e and T_e from line intensities, two different types of collisional-radiative-models can be used [9,10]. First, static "look-up" models, assume a collisional-radiative equilibrium (CRE), which allows a point-wise evaluation via line ratios and pre-calculated photo emission coefficients PEC(n_e, T_e). Second, dynamic models discard the CRE assumption and require a full description of the helium excitation states along the radial path of the injected neutrals [10,11].

In both cases, the accessible radial region is limited by the minimal required emission intensity of He I. Towards the plasma center, the amount of neutral helium drops due to ionization losses, whereas the emission in the far SOL is limited by low excitation rates due to low n_e and T_e. The limiting factor when applying a CRM is the low emission intensity of the 728 nm line, which is typically a factor of 10 weaker than that of the other lines [9].

For the standard evaluation of quasi-static n_e and T_e profiles, a relatively broad region can be accessed as the signal-to-noise ratio (SNR) is increased by averaging plasma profile measurements to about 1 ms (corresponding to an average of around 900 data points). This, however, hides the effect of single filaments and high frequency plasma modes.

For repetitive events like bursts, ELMs, or modes (cf. [12] for applied averaging in the I-mode regime), the SNR can be improved greatly by conditional averaging. Another option is the application of a linearized CRM for oscillating harmonic perturbations as described in [13]. With this approach, the amplitude of n_e and T_e fluctuations, as well as their cross-phase can be disentangled on short time scales. Due to the local linearization of the CRM, however, this method is only valid for a small pre-defined parameter range.

As discussed in this paper, the simplest method to access the spatiotemporal structure of modes and filaments is the direct interpretation of the measured line radiation, which can lead to the complications mentioned in the introduction. Therefore, one has to carefully choose the most viable analysis method to address different plasma phenomena with the He-beam diagnostic. In this paper we demonstrate that information about the mode frequency and spatial structure can be drawn from line ratios even without applying a CRM.

2.3. Radial localization of the measurement signal

Regardless of the analysis method used, a precise localization of the measured line radiation is crucial to the interpretation. In general, light is collected by an optical head along the whole path of the LOS. The advantage of active spectroscopy is that the light-emitting region is restricted to the overlap of the LOS with the injected neutral population. By applying forward models containing the 3D geometry, the emission distribution along the LOS can be exactly determined [7]. Chopping the neutral injection allows to subtract the contribution of passive background light. At AUG the passive contribution is typically a few percent of the total light. While the passive contribution can be easily subtracted from the active part for time averaged profile analysis, it might presents a complication for mode analysis. This is discussed in detail in Section 3.5.

Once the distribution of light emission along the line of sight is clarified, it has to be ensured that the results are not influenced by a radial smearing between excitation and emission of the injected neutrals or the above mentioned shadowing. Whereas the importance of shadowing is discussed in detail below, we show here, that radial smearing does not play a role for the thermal helium beam. The radial movement of the helium atoms between excitation and photon emission is typically <0.6 mm (the 706 nm line has the longest lifetime at 320 ns, $v_{He} = 1760$ m/s). The same holds for the total equilibration length (movement of the He atoms while the population of the spin system equilibrates with the local plasma parameters), which is typically also within the resolution of the diagnostic for densities higher than about 4×10^{18} m^{-3} (cf. [13, Appendix, Tab IV]).

This is different when signals of high energetic beams, as in alkali beam emission spectroscopy [14], are direct evaluated. The AUG Li-beam with 60 keV energy, for example, injects lithium with a velocity of 1290 km/s, which is approximately a thousand times faster compared to thermal helium. The lifetime of 27 ns of the 670.8 nm line thus leads to a radial smearing of 3.5 cm, as discussed in [15]. This smearing effect for alkali beams is well understood and needs to be taken into account for filament studies [14,15].

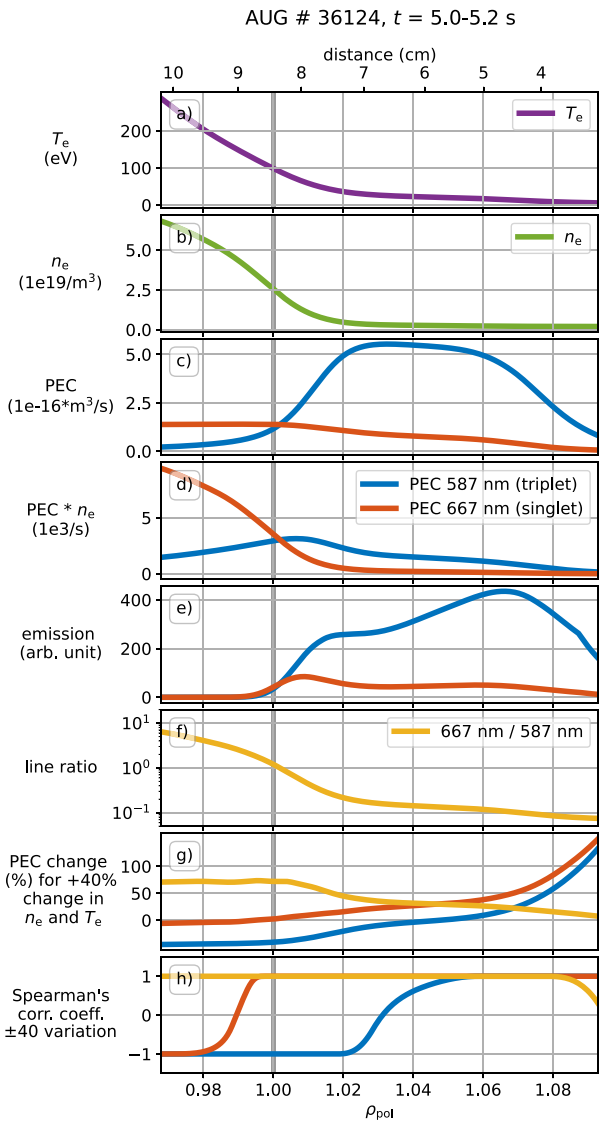

Fig. 1. Temperature (a) and density profile (b) from an AUG EDA H-mode discharge, averaged over 200 ms. The vertical gray line shows the separatrix position, given by the lower x-axis in ρ_{pol}. The upper x-axis shows the distance d to the helium injection point. The photo emission coefficients of the 587 nm and 667 nm lines (c), multiplied with n_e (d), and the neutral helium density leads to the total emission profile (e). The value of the line ratio is plotted in (f) and the local response of the line emission intensities and their ratio for a given +40% increase in n_e and T_e is shown in (g). (h) shows the Spearman's correlation coefficient of both line emissions and their ratio for a simultaneous change from minus to plus 40% percent of input n_e and T_e.

2.4. Influence of ionization on neutral distribution

Neutral ionization is a key factor for both the response of the total emission to n_e and T_e changes as well as the shadowing effect. To calculate the effective ionization of the neutrals, the exact neutral velocity is needed in addition to the plasma profiles (cf. Fig. 1(a), (b)) and ionization rates (cf. Fig. 2 a)). The mean velocity of helium in a Maxwell–Boltzmann distribution for room temperature is 1254 m/s as depicted in Fig. 2(d). As slow particles of the velocity distribution get ionized spatially before the fast ones, the mean value of the distribution along the injection path shifts towards higher values as shown in Fig. 2(e) and can exceed the thermodynamic limit of 1760 m/s for helium. The influence on the resulting ionization profile, i.e. the neutral fraction in Fig. 2(b), is small, as the neutral density drops fast in the region where this effect becomes most important. When supersonic velocity distributions are applied, as is the case for the gas source at AUG [10, Fig. 7], the radial change of the mean neutral velocity is even smaller, justifying the use of a constant velocity of 1760 m/s for the following analysis [10].

2.5. Non-linear connection between plasma parameters and line emission

When observing only one emission line the influence of changes in n_{He}, n_e or T_e on the emission, cannot be distinguished and simultaneous changes to multiple parameters cannot be disentangled. An increase in the emission in the far SOL, for example, is caused by higher excitation due to higher n_e, T_e, or both. In contrast to this, a rise of plasma pressure in the confined region typically leads to a signal drop. This can be explained by considering that the total line emission intensity I is given by

$$I = n_{He} \cdot n_e \cdot \mathrm{PEC}(n_e, T_e). \quad (1)$$

Fig. 1 shows n_e and T_e profiles (subplot (a), (b)) of an AUG EDA H-mode discharge, averaged over 200 ms so that the quasi-coherent mode is averaged out. Helium is injected from right to left, starting at a distance $d = 0$ (upper x-axis). To demonstrate the sensitivity and response of the helium beam diagnostics to n_e and T_e changes along the profile, we use the static CRM with photo emission coefficients (PEC) from ADAS as plotted in Fig. 1(c). The PECs (subplot (c) are not proportional to changes of n_e and T_e over the whole range. The triplet line at 587.6 nm reaches its relative population maximum already in the SOL at quite modest increases in electron temperature. For higher temperatures the PEC of the 587 nm line drops again, such that the line excitation further inwards becomes less efficient, even when the radially increasing electron density is taken into account (subplot (d). The helium density n_{He} drops quadratically with distance from the injection point and is further decreased due to ionization (Fig. 2(b)). According to (1), all three components together lead to the total line emission shown in Fig. 1(e).

This non-linear and non-monotonic relation between line emission and n_e and T_e for the various transitions is the reason for the differences in appearance of the emission patterns as presented in the next section. Under certain conditions this can even lead to a doubling of the measured oscillation frequency as discussed in [17, Figure 7.9] and visible in Fig. 3(d), (g) near the separatrix as well as in the spectrogram of Fig. 5 in the appendix. These effects, however, can be recognized by comparing the results of different emission lines or taking line ratios for the analysis. When a linear response of the signal to n_e and T_e changes is of interest, the singlet/triplet ratio of the 667.8 nm and 587.6 nm lines is a favorable choice for mode analysis around the separatrix, as plotted in Fig. 1(f). This ratio depends only on the PECs from Fig. 1(c) and thus is the same for Fig. 1(c)–(e), as n_e and n_{He} cancel out.

Next to a linear response, the selected line ratio also shows a high sensitivity to changes of n_e and T_e. This is shown in Fig. 1(g), where the line ratio change is compared to the PEC change of both individual lines for a 40% increase of the local n_e and T_e values. It can be seen, that the line ratio change is positive over the whole radius and highest at the plasma edge. Individual lines show a strong positive response in the far SOL, making the analysis of one wavelength a suitable tool for filament studies [18]. In the near SOL and separatrix regions, however, the response of these lines is small or gets inverted, so that they do not, alone, deliver a proper picture of the plasma dynamics in this region.

A broader picture on how the individual lines and their ratio react on plasma perturbation is given in the Spearman correlation plot Fig. 1 h) [19]. This measure of rank correlation shows how well the relationship between variables, in this case the change of n_e and T_e and their effect on emission, can be described with a monotonic function. For this example, n_e and T_e were varied locally by ±40% percent to calculate the correlation coefficient. We see that the line ratio shows always a positive correlation with the plasma dynamics, whereas the correlation of individual lines becomes negative towards the plasma center. This

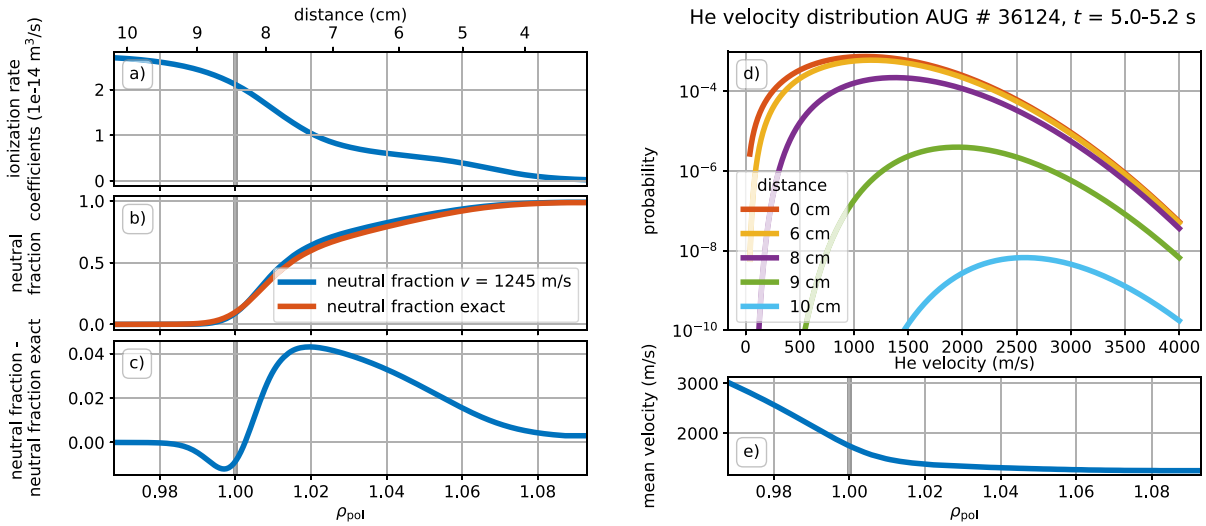

Fig. 2. This figure shows how the locally injected neutral helium for active spectroscopy is ionized along its propagation path. The helium is injected from right to left, starting at the distance zero (see upper x-axis). The ionization rates coefficients (a) from the ADAS file 'scd96_he.dat' [16] correspond to the plasma profiles shown in Fig. 1. Subplot (b) compares the effective neutral fraction for a constant single velocity of $v = 1245\,\mathrm{m/s}$ to the different ionization taking a thermal velocity distribution and its change along the propagation path into account. The small difference between both approaches from (b) is plotted in (c). The change of the velocity distribution along the injection path is shown in (d). As slow atoms in the distribution are ionized earlier, the mean propagation velocity increases along the path as plotted in (e).

generally happens earlier for triplet lines, compared to singlet lines. The reason therefore is that the response becomes negative once the absolute emission maximum is passed, which lies further outwards for triplet lines compared to singlet lines as plotted in Fig. 1(e).

3. Interpretation of modeled and measured emission data on short time scales

3.1. Input parameters for the systematic diagnostic

The general dependencies of line emission changes due to changes in n_e and T_e along the radial profile were discussed in the last section. In this section we highlight the implications of non-linear emission responses and the shadowing effect on the interpretation of spatial structures of the high frequency quasi-coherent mode (QCM), which is characteristic for the ELM free EDA H-mode [5,20]. The QCM shows typical frequencies of 15–70 kHz and is prominently visible in reflectometer signals, the electron-cyclotron-emission (ECE) diagnostic as well as in the emission data of the thermal helium beam. The mode dominates the plasma dynamics in the vicinity of the separatrix and is thought to favor filament generation. These intermittent filaments dominate the transport in the far SOL [18], as discussed in the next subsection.

To demonstrate the misleading diagnostics effects, experimental data are compared to a synthetic helium beam diagnostic for an EDA H-mode scenario (# 36 124, t = 5–5.2 s, $P_{\mathrm{ECRH}} = 1.65\,\mathrm{MW}$, $n_{\mathrm{core}} = 8 \times 10^{19}\,\mathrm{m}^{-2}$). To set up the synthetic diagnostic we first assume steady state n_e and T_e background profiles as given in Fig. 1(a) and (b). We then add a 40% in-phase fluctuation of n_e and T_e with a frequency of 29 kHz restricted to a radial region from $\rho_{\mathrm{pol}} = 0.99$–$1.01$, with ρ_{pol} being the normalized poloidal magnetic flux coordinate. Although a more physical description of the mode amplitude along the plasma radius leads to an even better match of experimental and modeled results, the model with a constant relative fluctuation level within a fixed interval is designed to best demonstrate the shadowing effect. The appearance of SOL filaments, also included in the model, is discussed in Section 3.4.

3.2. Signal normalization

For direct visualization and tracking of plasma fluctuations at the plasma edge, a signal normalization is useful. Within a time span, the signal I is normalized for each radial channel separately by first subtracting the minimum of the signal and then dividing it by the signal maximum:

$$I_{\mathrm{norm}} = \frac{I - \min(I)}{\max(I - \min(I))}. \tag{2}$$

This results in values between zero and one for each radial location, which corresponds to relative signal changes without taking the absolute signal value into account. The resulting normalized signal of the model input n_e is plotted in Fig. 3(a). It shows the QCM around the separatrix as well as the filaments propagating in the SOL. This enables the direct calculation of the radial propagation velocity of SOL filaments by extracting the slope of the filament trajectory [18]. To be able to perform this normalization with the input data of the model, noise was added to the input n_e and T_e values in order to avoid division by zero. With this normalization a noisy region, as in Fig. 3(a) for a distance >9 cm, indicates a signal purely dominated by noise, without the presence of bursts or periodic perturbations.

3.3. Interpretation of mode structures

The density input for the synthetic diagnostic is shown in Fig. 3(a). To calculate the ionization of the injected helium, the spatiotemporal input data are transferred into the frame of the inward moving helium atoms with a velocity of 1760 m/s. This leads, in the lab-frame, to the neutral He distribution in subplot (b), where the path of a helium atom (starting at $t = 0$ at the helium injection point $d = 0$), is indicated with red arrows. This time dependent neutral distribution is the source of the shadowing effect. The periodic increase and decrease of neutral ionization at the mode location is carried inwards by the propagating He atoms. This leads to a time-shifted variation of the neutral He density further inwards and thus to a modulation of the triplet (c) and singlet (d) line emission intensity, visible in regions of $\rho_{\mathrm{pol}} < 0.99$, where the mode is not present in the input signal.

This clearly demonstrates that the local presence of a mode cannot always be deduced from local modulated light emission, as usually done in GPI on a single emission line. While the demarcation of the outer radial range of mode activity is easily possible, line ratios must be used for the demarcation of the inner boundary. Fig. 3(e) shows this line ratio, where the influence of the neutral distribution, i.e. the He density, cancels out. The shadowing effect is eliminated and the ratio reflects the correct spatiotemporal structure of the mode, due to

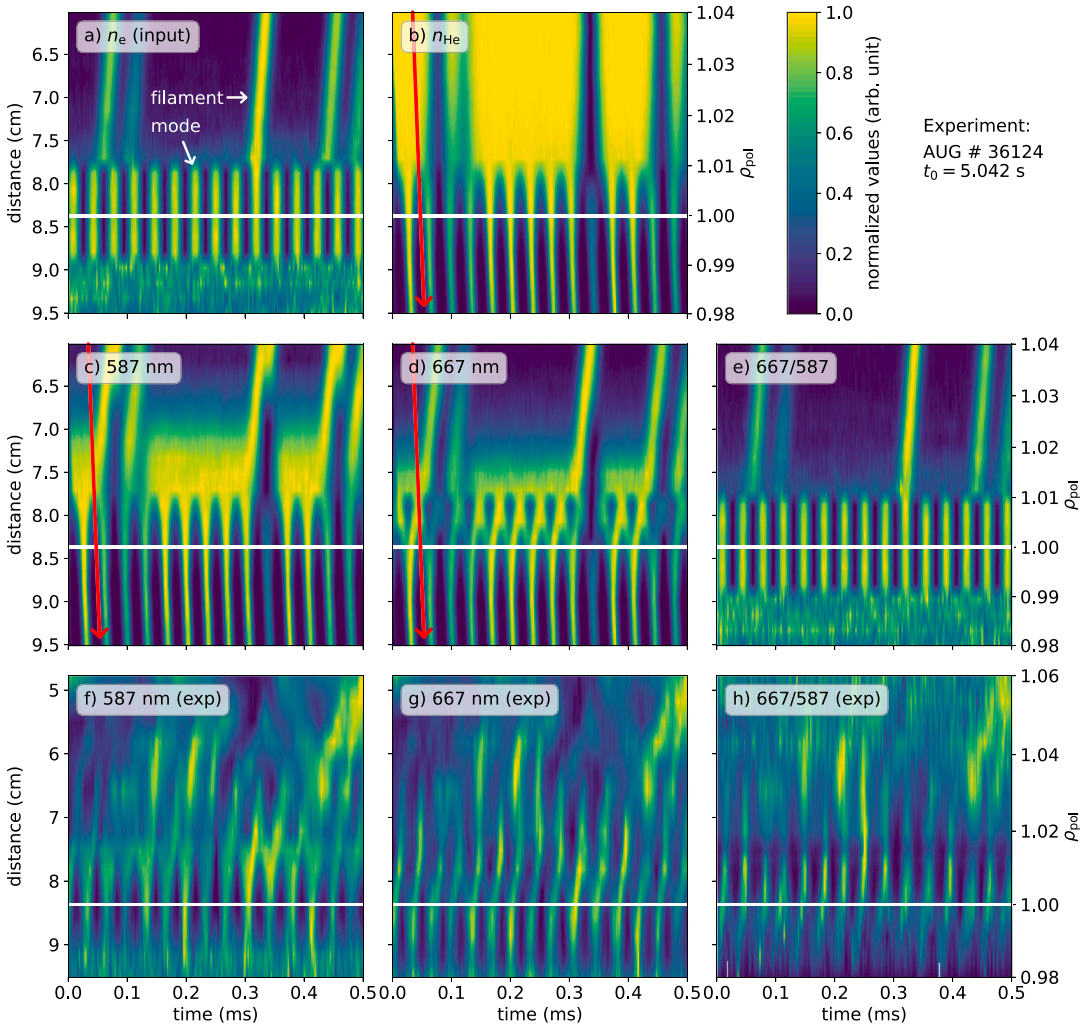

Fig. 3. Modeled (a)–(e) and experimental (f)–(h) data of an AUG EDA H-mode discharge for a 5 ms long time window, showing the 29 kHz QCM around the separatrix and five filaments in the SOL region. (a) shows exemplary n_e as the input of the synthetic diagnostic. T_e is not shown as it looks identical to n_e due to the normalization. n_e and T_e input are used to generate the neutral helium distribution (b) along the helium injection path starting at a distance zero. The red arrow indicates the trajectory of an injected He atom with 1760 m/s. Both, the modeled (c), (d) and experimental (f), (g) emission data show features, which can be removed when line ratios (e), (h) are used for analyzing mode structures. The white horizontal line denotes the last closed flux surface (separatrix) at $\rho_{pol} = 1.0$.

the linear response to plasma fluctuations as discussed in the previous section. Hence, the pattern of Fig. 3(e) resembles the one of Fig. 3(a), while the patterns given by individual emission lines (panels (c) and (d)) show clear differences with respect to the input.

The mode in the model has a constant radial phase over its whole range, which corresponds to a radial wavenumber vector $k_r = 0$ [21]. This is correctly represented in the line ratio, but not in the data from individual emission lines as visible in Fig. 6 in the appendix, which shows calculated k_r values for the simulated data along the radius. In the region of $\rho_{pol} < 0.99$ with no mode activity, the shadowing effect and the resulting emission structure leads to false values of $k_r \approx -1\,\mathrm{cm}^{-1}$. This is connected to the inwards propagation of the neutrals with a velocity $v = 2\pi f / k_r$. Correctly, no k_r value can be assigned for the line ratio in this region.

Interpreting the visible tilt of the structure, in the region where the mode is active, would also lead to false values of $k_r \neq 0$. This artificial tilt is caused by a combination of the shadowing effect (dominant in Fig. 3(c) over the whole domain) and the response of the line emission to n_e and T_e changes as discussed in Section 2.5 (dominant in Fig. 3(d) around the separatrix).

As displayed in Fig. 1(h) the response of the triplet line to n_e and T_e changes is negative for $\rho_{pol} < 1.03$, i.e. in the whole region of the mode. Therefore, the emission modulation in Fig. 3(c) starts already in anti-phase to the mode at $\rho_{pol} = 1.01$, as an increase of n_e and T_e leads to a lowering of the emission. In contrast to this, the singlet line response is positive in the whole SOL. Therefore, the emission change in the SOL of the singlet line in Fig. 3(d) starts in-phase with the mode, whereas inside the separatrix the emission is in anti-phase to the mode due to the modulated He density being dominant. In the transition region close to the separatrix in the near SOL, a doubling of the frequency can be observed.

As all these effects vanish for the line ratio in Fig. 3e, it is shown that information about the mode frequency and localization can be drawn reliably from line ratios.

The same dynamics of the modeled data can be seen in the experiment (Fig. 3(f)–(h)), where the different characteristics of singlet and triplet lines can be clearly recognized.

3.4. Appearance of SOL filaments

In the experiment, filaments spread into the far SOL, possibly generated by the high frequency mode, which enables transport across the shear layer. This might explain why the filament rate in EDA H-modes is higher compared to regimes without the presence of strong mode activity [18].

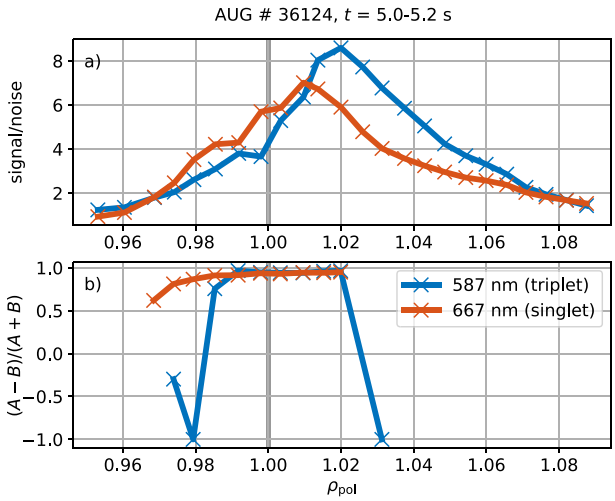

Fig. 4. Measures for the signal quality of the 587 nm and 667 nm emission lines along the radius of an AUG EDA H-mode scenario. (a) represents the SNR and (b) the relative mode amplitude between active (A) and background (B) phases. The markers denote the measurement locations.

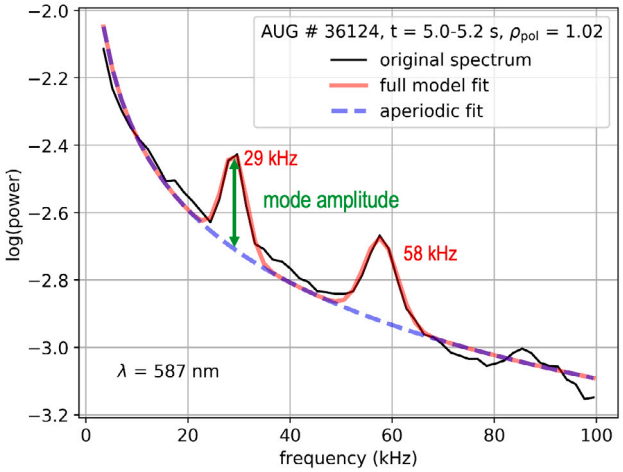

Fig. 5. Spectrum of the QCM with a peak frequency of $f = 29$ kHz for the spectral line at $\lambda = 587$ nm. This line also shows the mode with its double frequency of $f = 58$ kHz at $\rho_{pol} = 1.02$, as discussed in Section 2.5. The fit model to calculate the aperiodic (noise) and periodic (mode) components of the spectrum is described in [23].

In the input for the synthetic diagnostic, five SOL filaments are randomly placed within the given time interval. The filament behavior was chosen to demonstrate diagnostic effects in a typical parameter range, inspired by experiment [14,22]. In Fig. 3 filaments start at the separatrix with the local n_e and T_e value at their birth moment. They propagate radially outwards with 1 km/s. During their propagation path from the separatrix on outwards they linearly lose 70% of their initial n_e and T_e values until they reach the end of the simulation domain at $\rho_{pol} = 1.04$. This leads to plasma fluctuation amplitudes exceeding 100% in the far SOL.

In contrast to the mode in the high n_e and T_e region, SOL filaments show a similar appearance, independent of the analyzed wavelength. This is explained with Fig. 1(g) and (h), showing the positive response of the photo emission onto n_e and T_e increase in the SOL. This holds because the additional ionization by filaments in the far SOL is typically of minor importance. It leads to a slight intensity loss in the shadow of the filament and thus also to a slight shift of the emission peak in respect to the filament position, but without changing the complete appearance of filaments.

3.5. Reliability boundaries

It was demonstrated that the location and spatiotemporal structure of modes around the separatrix are best reflected when line ratios are used for the analysis. The experimentally accessible range towards the plasma center, however, is limited by the rapidly decreasing He density and thus the low emission.

In this region, the passive background light might become decisive, as an apparent wrong offset of one emission line distorts intensity ratios. An apparent, but wrong signal offset can appear when the background intensity is not constant over short time scales. This is the case, when the mode structure is also visible in the non-localized background, which contains contributions from all along the LOS including regions from outside the actively puffed helium cloud. Therefore, an experimental approach is needed to rate the reliability boundary in the low signal region towards the plasma center.

As first qualifier for mode localization, we have a look onto the signal-to-noise ratio (SNR) of the diagnostic. It is calculated by the background corrected signal divided by its standard deviation (std). Before calculating the std, the impact of the periodic QCM is removed from the signal by applying a band-stop filter of ±10 kHz around the peak frequency of the QCM and ±5 kHz around its first harmonics. The resulting SNR values are plotted in Fig. 4(a) along ρ_{pol}. The SNR is highest in the near SOL. In the far SOL, the SNR decreases as the std is increased by non-coherent plasma perturbations, i.e. filaments, which appear like strong spikes on the signal [18]. Towards the innermost measurements channels, the SNR drops due to the low emission and the signal gets dominated by photon noise, hampering a precise mode demarcation.

As second qualifier, the mode amplitude of active (A) and background phases (B) are compared to ensure that the fluctuation amplitude of the signal is not dominated from contributions of the non-localized background. In order to extract the amplitude of the periodic mode laying on top of the aperiodic noise contributions of the signal spectrum, the method described in [23] is used for signal and background phases separately. This is illustrated in Fig. 5 for a signal of the 587 nm line in the near SOL, where the mode is visible with the main and doubled frequency. As qualifier for a localized mode measurement, the normalized quantity $(A-B)/(A+B)$ is plotted in Fig. 4 b). In regions where the mode is neither visible in the signal nor in the background, i.e. $A + B = 0$, the qualifier is not defined.

From this analysis it can be learned, that the mode visibility in the 587 nm line for $\rho_{pol} \leq 0.98$ is restricted by the low emission. In the 667 nm line it is visible further inwards as the singlet line has a higher SNR in the confined region. Because a good signal of two lines is needed for line ratios which cancel the shadowing effect, a proper demarcation of the mode activity towards the plasma center is not possible in the given example. The spatiotemporal structure of the mode plotted in Fig. 3(h) for $\rho_{pol} > 0.98$, however, is shown to arise from localized measurements and thus can be interpreted reliably with the given line ratio.

4. Conclusion

In this paper data from the thermal helium beam diagnostic at ASDEX Upgrade in an EDA H-mode scenario are compared to a synthetic diagnostic model to reveal diagnostic effects. It highlights the influence of ionization losses on the neutral helium distribution. These neutral losses are carried inwards by the radially injected helium which transits the relevant radial region on similar time scales to turbulent processes and filament motion. The result is a shadowing effects which prevents the localization of turbulent structures if only one spectral line is analyzed. Furthermore, it is shown that the emission response of individual lines does not directly correlate with changes of plasma

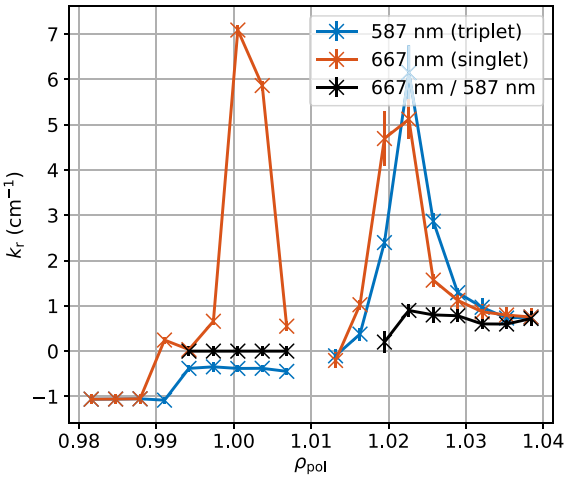

Fig. 6. Radial wavenumber k_r of the simulated emission data in Fig. 3(c), (d) for individual emission lines and e) for the line ratio. Whereas the line ratio matches the input of $k_r = 0$ at the region of the mode, individual lines show wrong k_r values. Due to the shadowing effect, finite k_r values of $k_r \approx -1\,\mathrm{cm}^{-1}$ are even calculated in regions $\rho_{pol} < 0.99$. Finite values of k_r for $\rho_{pol} > 1.01$ are caused by filaments.

n_e and T_e at typical plasma parameters around the separatrix and in the confined region.

Relying on the linear response of one emission line can thus lead to false interpretation of the data. We demonstrate that this false interpretation can be prevented when the ratio of two helium emission lines is used for the analysis. It is further shown, that in regions of very low emission intensity at the edge of the diagnostic applicability, an accurate background subtraction is crucial to maintain the accuracy of the diagnostics.

Taking all these effects into account we show that by analyzing line intensities and their ratios, determining the shape, size, frequency and localization of turbulent structures is precisely possible. Therefore, the results of this work are highly important for active spectroscopy such as thermal helium beam spectroscopy or gas puff imaging.

CRediT authorship contribution statement

M. Griener: Conceptualization, Methodology, Software, Formal analysis, Writing – original draft, Writing – review & editing, Visualization, Data curation. **J. Kalis:** Software, Formal analysis, Partial writing, Visualization. **D. Wendler:** Software, Formal analysis, Data curation. **G. Birkenmeier:** Conceptualization, Validation. **E. Wolfrum:** Methodology, Validation. **R.M. McDermott:** Methodology, Proof reading, Validation. **U. Stroth:** Project administration, Funding acquisition. **ASDEX Upgrade Team:** Funding acquisition. **EUROfusion MST1 Team:** Funding acquisition.

Declaration of competing interest

The authors declare that they have no known competing financial interests or personal relationships that could have appeared to influence the work reported in this paper.

Data availability

Data will be made available on request.

Acknowledgments

This work has been carried out within the framework of the EUROfusion Consortium, funded by the European Union via the Euratom Research and Training Programme (Grant Agreement No 101052200 — EUROfusion). Views and opinions expressed are however those of the author(s) only and do not necessarily reflect those of the European Union or the European Commission. Neither the European Union nor the European Commission can be held responsible for them.

J. Kalis, D. Wendler and G. Birkenmeier received funding from the Helmholtz Association, Germany under Grant No. VH-NG-1350.

Appendix A

See Figs. 5 and 6

References

[1] S.J. Zweben, J.L. Terry, D.P. Stotler, R.J. Maqueda, Invited review article: Gas puff imaging diagnostics of edge plasma turbulence in magnetic fusion devices, Rev. Sci. Instrum. 88 (4) (2017) 41101.

[2] D.P. Stotler, B. LaBombard, J.L. Terry, S.J. Zweben, Neutral transport simulations of gas puff imaging experiments, J. Nuclear Mater. 313–316 (SUPPL.) (2003) 1066–1070.

[3] D.P. Stotler, S. Ku, S.J. Zweben, C.S. Chang, R.M. Churchill, J.L. Terry, Shadowing effects in simulated Alcator C-Mod gas puff imaging data, Nucl. Mater. Energy 19 (2019) 113–119.

[4] A. Coroado, P. Ricci, Numerical simulations of gas puff imaging using a multi-component model of the neutral–plasma interaction in the tokamak boundary, Phys. Plasmas 29 (3) (2022) 032511.

[5] L. Gil, C. Silva, T. Happel, G. Birkenmeier, G.D. Conway, L. Guimarais, A. Kallenbach, T. Pütterich, J. Santos, P.A. Schneider, M. Schubert, E. Seliunin, A. Silva, J. Stober, U. Stroth, E. Trier, E. Wolfrum, Stationary ELM-free H-mode in ASDEX upgrade, Nucl. Fusion 60 (5) (2020) 054003.

[6] M. Griener, O. Schmitz, K. Bald, D. Bösser, M. Cavedon, P. De Marné, T. Eich, G. Fuchert, A. Herrmann, A. Kappatou, T. Lunt, V. Rohde, B. Schweer, M. Sochor, U. Stroth, A. Terra, E. Wolfrum, Fast piezoelectric valve offering controlled gas injection in magnetically confined fusion plasmas for diagnostic and fuelling purposes, Rev. Sci. Instrum. 88 (3) (2017) 33509.

[7] M. Griener, E. Wolfrum, M. Cavedon, R. Dux, V. Rohde, M. Sochor, J.M. Muñoz Burgos, O. Schmitz, U. Stroth, Helium line ratio spectroscopy for high spatiotemporal resolution plasma edge profile measurements at ASDEX upgrade (invited), Rev. Sci. Instrum. 89 (10) (2018) 10D102.

[8] G. Fuchert, G. Birkenmeier, D. Carralero, T. Lunt, P. Manz, H.W. Müller, B. Nold, M. Ramisch, V. Rohde, U. Stroth, Blob properties in L- And H-mode from gas-puff imaging in ASDEX upgrade, Plasma Phys. Control. Fusion 56 (12) (2014) 125001.

[9] M. Griener, J.M. Burgos, M. Cavedon, G. Birkenmeier, R. Dux, B. Kurzan, O. Schmitz, B. Sieglin, U. Stroth, E. Viezzer, E. Wolfrum, Qualification and implementation of line ratio spectroscopy on helium as plasma edge diagnostic at ASDEX upgrade, Plasma Phys. Control. Fusion 60 (2) (2018) 025008.

[10] D. Wendler, R. Dux, R. Fischer, M. Griener, E. Wolfrum, G. Birkenmeier, U. Stroth, Collisional radiative model for the evaluation of the thermal helium beam diagnostic at ASDEX upgrade, Plasma Phys. Control. Fusion 64 (4) (2022) 045004.

[11] J.M. Muñoz Burgos, M. Griener, J. Loreau, A. Gorbunov, T. Lunt, O. Schmitz, E. Wolfrum, Evaluation of emission contributions from charge-exchange between the excited states of deuterium with He+ during diagnostic of thermal helium gas beam injection and laser-induced fluorescence, Phys. Plasmas 26 (6) (2019) 063301.

[12] T. Happel, M. Griener, D. Silvagni, S.J. Freethy, P. Hennequin, F. Janky, P. Manz, D. Prisiazhniuk, F. Ryter, M. Bernert, D. Brida, T. Eich, M. Faitsch, L. Gil, L. Guimarais, A. Merle, D. Nille, J. Pinzón, B. Sieglin, U. Stroth, E. Viezzer, Stationarity of I-mode operation and I-mode divertor heat fluxes on the ASDEX Upgrade tokamak, Nucl. Mater. Energy 18 (2019) 159–165.

[13] T. Nishizawa, M. Griener, R. Dux, G. Grenfell, D. Wendler, S. Kado, P. Manz, M. Cavedon, Linearized spectrum correlation analysis for thermal helium beam diagnostics, Rev. Sci. Instrum. 92 (10) (2021).

[14] G. Birkenmeier, F.M. Laggner, M. Willensdorfer, T. Kobayashi, P. Manz, E. Wolfrum, D. Carralero, R. Fischer, B. Sieglin, G. Fuchert, U. Stroth, Magnetic field dependence of the blob dynamics in the edge of ASDEX upgrade L-mode plasmas, Plasma Phys. Control. Fusion 56 (7) (2014) 075019.

[15] M. Willensdorfer, G. Birkenmeier, R. Fischer, F.M. Laggner, E. Wolfrum, G. Veres, F. Aumayr, D. Carralero, L. Guimarãis, B. Kurzan, Characterization of the Li-BES at ASDEX Upgrade, Plasma Phys. Control. Fusion 56 (2) (2014) 25008.

[16] H.P. Summers, The ADAS User Manual, version 2.6, 2004.

[17] M. Griener, Active line ratio spectroscopy on thermal helium at ASDEX upgrade (Ph.D. thesis), Technische Universität München, 2018, p. 128.
[18] M. Griener, E. Wolfrum, G. Birkenmeier, M. Faitsch, R. Fischer, G. Fuchert, L. Gil, G.F. Harrer, P. Manz, D. Wendler, U. Stroth, Continuous observation of filaments from the confined region to the far scrape-off layer, Nucl. Mater. Energy 25 (2020) 100854.
[19] C. Spearman, Demonstration of formulae for true measurement of correlation, Am. J. Psychol. 18 (2) (1907) 161.
[20] C. Theiler, J.L. Terry, E. Edlund, I. Cziegler, R.M. Churchill, J.W. Hughes, B. LaBombard, T. Golfinopoulos, Radial localization of edge modes in Alcator C-Mod pedestals using optical diagnostics, Plasma Phys. Control. Fusion 59 (2) (2017) 025016.
[21] J. Cheng, J. Dong, K. Itoh, S.-I. Itoh, L. Yan, X. Zhiqiang, M. Jiang, Z. Huang, K. Zhao, S. Zhongbing, W. Zhong, S. Inagaki, T. Kobayashi, K. Ida, Y. Kosuga, M. Sasaki, M. Han, Z.-X. Wang, M. xu, Y. Xu, Formation of radially elongated flow leading to onset of type-III edge localized modes in toroidal plasmas, Nucl. Fusion 60 (2020).
[22] M. Kočan, F.P. Gennrich, A. Kendl, H.W. Müller, Ion temperature fluctuations in the ASDEX Upgrade scrape-off layer, Plasma Phys. Control. Fusion 54 (8) (2012) 085009.
[23] T. Donoghue, M. Haller, E.J. Peterson, P. Varma, P. Sebastian, R. Gao, T. Noto, A.H. Lara, J.D. Wallis, R.T. Knight, A. Shestyuk, B. Voytek, Parameterizing neural power spectra into periodic and aperiodic components, Nature Neurosci. 23 (12) (2020) 1655–1665.